Journal of Power Sources 195 (2010) 3130–3134

Contents lists available at ScienceDirect

Journal of Power Sources

journal homepage: www.elsevier.com/locate/jpowsour

Short communication

Effect of zinc oxide on yttria doped ceria

Ling Gao, Ming Zhou, Yifeng Zheng, Haitao Gu, Han Chen, Lucun Guo*

College of Material Science and Engineering, Nanjing University of Technology, No. 5 Xinmofan Road, Nanjing, Jiangsu, 210009, PR China

ARTICLE INFO

Article history:
Received 12 October 2009
Received in revised form
18 November 2009
Accepted 25 November 2009
Available online 1 December 2009

Keywords:
Solid oxide fuel cell
Yttria doped ceria
Zinc oxide
Sintering aid

ABSTRACT

Solid electrolyte ceramics consisted of ceria, yttria and zinc oxide has been synthesized through solid state reaction. With the zinc oxide content over 0.4 mol.%, this material is able to achieve a relative density of 96% at 1375 °C, about 200 °C lower than that without zinc oxide. The result of XRD reveals that the lattice parameter increased with the concentration of zinc oxide up to 0.6 mol%, suggesting its solubility limit for fluorite structure of ceria. It is also found that this doping level is coincident with that where it has the highest ionic conductivity. Furthermore, it is detected by EDS that the excess zinc oxide tends to agglomerate and locate on the surface of sintered sample when the addition exceeds the solubility limit.

1. Introduction

Fluorite structure oxides such as zirconia, ceria and thoria are found to be good oxygen conductors and widely used in solid oxide fuel cell (SOFC), oxygen sensor or other electrochemical devices [1,2]. During the last decades, fully stabilized zirconia was the most commonly applied electrolyte for SOFC. However, its high operating temperature (800–1000 °C) leads to a severe criteria for other fuel cell components. Hence, intensive studies have been done on alternative electrolyte for intermediate temperature (500–800 °C) SOFC (IT-SOFC). Because of the relatively higher ionic conductivity and lower interfacial losses with electrode, ceria-based electrolyte has drew much attention [3–11].

Pure stoichiometric ceria holds the fluorite structure with space group of Fm3m over the whole temperature range from room temperature to its melting point. This structure is of considerable tolerance to the dissolution of other oxides. Generally, excess oxygen vacancies are generated by doping alkaline-earth and rare-earth oxides of lower valences

$$M_2O_3 \xrightarrow{CeO2} 2M'_{Ce} + V_O^{\bullet\bullet} + 3O_O \quad (1)$$

The relative high values for ionic conduction were observed with Sm, Gd and Y as acceptor dopants [3–5]. Considering the abundance of these rare-earth elements, yttria doped ceria (YDC) is a potentially low-cost electrolyte for IT-SOFC.

Electrical properties of YDC had been well investigated. Both Wang and Bryan Balazs' group measured the ionic conductivity as a function of yttria concentration and declared an optimum composition as 8 mol.% yttria doped ceria [5,12]. Since the electrolyte materials are usually co-sintered with other cell components to avoid the warps and cracks stemming from shrinkage differences, lower sintering temperature (<1400 °C) is desired to restrain solid state reactions, diffusions between ceramic materials and other serious problems. However, as the result of the refractory nature, fabrication of such YDC bulk ceramics below 1550 °C is still a challenge for its application in IT-SOFC [13–15].

So far, researches on low temperature sintering of ceria-based materials have mainly focused on searching suitable sintering aid for solid reaction process or synthesis of highly reactive ceramics powder. For the sintering aid, CoO, MnO, Al_2O_3 and CuO were found effectively improving the densification but they showed detrimental influence on conductivity [16–21]. For the powder synthesis, nanosized YDC powder with low agglomeration was obtained by gel combustion method [22–27]. Nevertheless, compared with conventional solid state reaction method, this route involves pH value controlling, concentration selection and other extra procedures.

In the present work, zinc oxide was demonstrated as an appropriate sintering aid for YDC. The density and ionic conductivity of the co-doped specimens were also investigated in detail.

2. Experimental procedure

2.1. Sample preparation

Series of solid solutions with general formula $(Ce_{0.84}Y_{0.16}O_{1.92})_{1-x}(ZnO)_x$ with $x = 0$, 0.2 mol.%, 0.4 mol.%, 0.6 mol.%, and 0.8 mol.% (noted as YDC0Zn–YDC0.8Zn) were synthesized through solid state reaction process. Commercial ceria

* Corresponding author. Tel.: +86 025 83587261; fax: +86 025 83306152.
E-mail address: lc-guo@163.com (L. Guo).

0378-7753/$ – see front matter © 2009 Elsevier B.V. All rights reserved.
doi:10.1016/j.jpowsour.2009.11.117

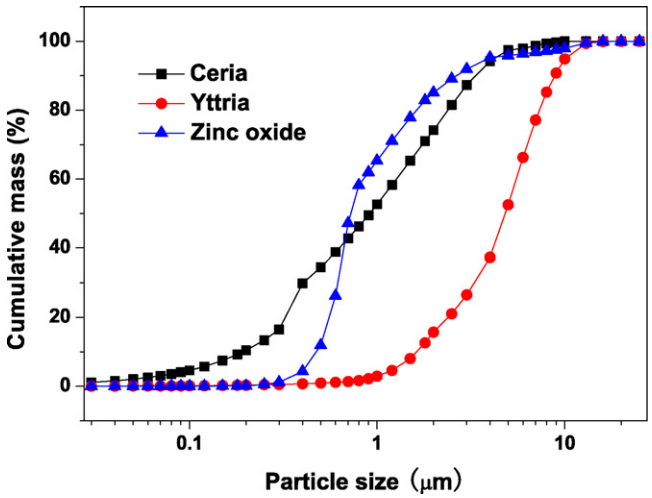

Fig. 1. Particle distribution of starting materials.

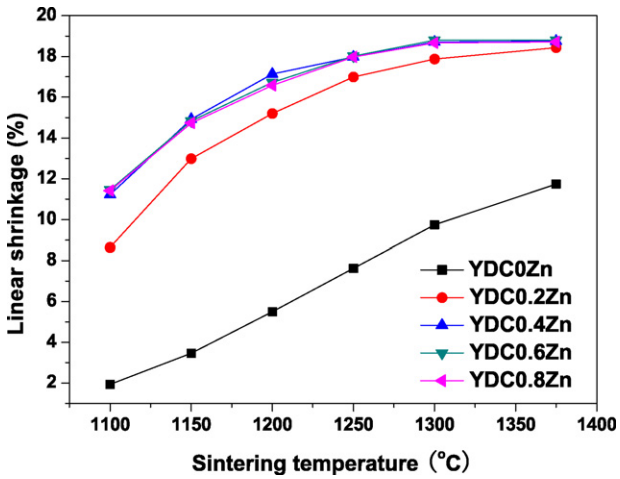

Fig. 2. Linear shrinkage vs. sintering temperature for YDC with different zinc oxide contents.

powder (99.5% pure, Yixing Xinwei Leeshing Rare Earth Co., Ltd., China), yttria powder (99.9% pure, Yixing Xinwei Leeshing Rare Earth Co., Ltd., China) and zinc oxide powder (99.5% pure, Shanghai Chemical Reagent Plant, China) were used as starting materials. The raw powders were carefully measured according to the desired proportion and milled with distilled water for 10 h, using yttria stabilized zirconia balls as milling media in a planetary mill. After drying, the powders were ground and axially die pressed into cylindrical pellets (21.5 mm in diameter and 1.7 mm in thickness) under a pressure of 85 MPa. These green bodies were heated at 3 °C min^{-1} to various temperatures (1300–1600 °C), soaked for 20 h, and subsequently cooled to the room temperature.

2.2. Characterization

The particle size distributions of raw oxide powders were determined by NSKC-1 Photo Size Analyzer (NJUT, China), and the result was shown in Fig. 1. The mean particle size (D50) of ceria, yttria and zinc oxide is 0.914 μm, 4.827 μm and 0.725 μm, respectively. Densities of sintered pellets were determined by Archimede's method by immersing the samples in distilled water. Crystal structures were identified at room temperature by D/Max-RB X-ray diffractometer (Rigaku, Japan) with Cu Kα radiation in the 2θ range of 20–90°. The cross-sections and surfaces of samples were observed by JSM-5900 (JEOL, Japan) and S3400N (HITACHI, Japan) scanning electron microscope (SEM).

For electrical measurements, silver paste was applied on both sides of the pellets and baked at 700 °C for 10 min. The as-prepared samples were mounted in an alumina supporter and jigged with Pt wires by ceramic springs. AC impedance analyses were carried on in the air between 400 °C and 800 °C at intervals of 50 °C over the frequency range of 0.1 Hz to 10 MHz using PARSTAT2273 frequency response analyzer (AMETEK, US). The data of complex impedance were fitted by software ZSimpwin according to the equivalent circuits proposed by Van Dijk and Burggraaf for the brick-layer model at different temperature regions [28].

3. Results and discussion

3.1. Shrinkage and densification

The difference in sintering behavior between pure YDC and ZnO added samples is particularly evident from the linear shrinkage curves which were presented in Fig. 2. A enhancement of sintering procedure was observed with ZnO content up to 0.4 mol.%; addition above this level had no further effect on the shrinkage. In the range of 1100–1375 °C, the modified systems with ZnO concentration above 0.4 mol.%, achieved a certain shrinkage degree at a temperature 300 °C lower compared with the pristine YDC. Moreover, they all obtained their maximum shrinkage (~18.7%) at 1375 °C, whereas it is only 11.7% for YDC.

Fig. 3 showed the calculated relative densities of the samples sintering at various temperatures with soaking time of 20 h. The specimens with ZnO amount above 0.4 mol.% achieved the peak value (~96%) at 1375 °C, meanwhile it is only 60% of theoretical density for YDC0Zn. It is noted that this decreased sintering temperature is of the same degree with the samples prepared by nanosized raw powder [28].

3.2. Phase composition and crystal structure

The XRD patterns of the specimens sintering at 1375 °C (YDC0Zn at 1600 °C) for 20 h were shown in Fig. 4. It can be seen that, for the pressing condition and sintering regime, only single phase of ceria with Fm3m cubic fluorite structure was identified in all the compositions. Lattice parameter of each sample was obtained by fitting the peak data using software Jade. The impact of ZnO content on it was presented in Fig. 5. The lattice parameter decreases with increasing ZnO concentration from 5.4075 Å to 5.4054 Å when the doping level is lower than 0.6 mol.%, and then retains constant with

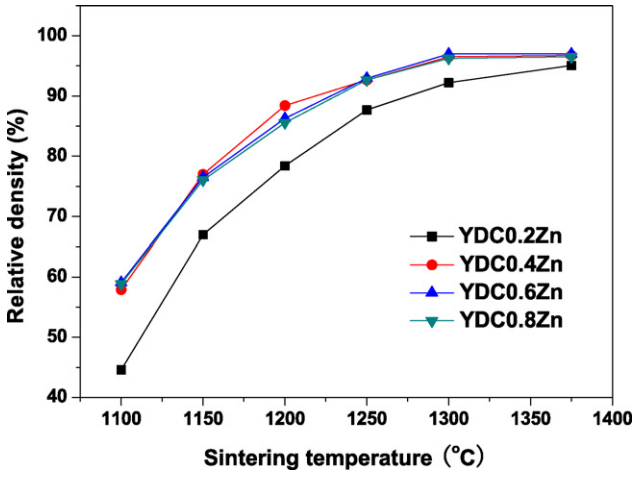

Fig. 3. Relative density vs. sintering temperature for YDC with different zinc oxide contents.

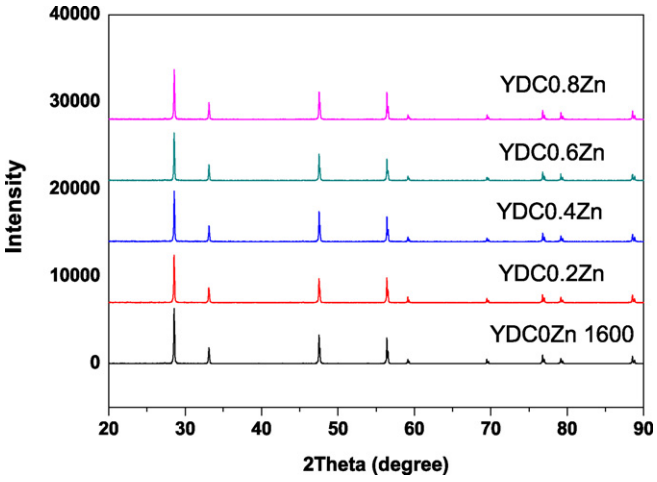

Fig. 4. XRD patterns of YDC with different zinc oxide contents.

continued addition. Since the ionic radii of Ce^{4+}, Y^{3+}, and Zn^{2+} are 0.97 Å, 1.019 Å and 0.9 Å respectively [29], we speculated that there may exit a substitutional solid solution as the Ce^{4+} was replaced by the smaller Zn^{2+} cation. Using Kroeger–Vink notation, the reaction can be expressed as:

$$ZnO \xrightarrow{CeO_2} Zn''_{Ce} + O^{\times}_{O} + V^{\bullet\bullet}_{O} \quad (2)$$

when one mole of ZnO dissolves into ceria, there form a negative charged divalent substituted zinc site and a positive charged divalent oxygen vacancy. And it is implied by the lattice parameter that the solid solubility limit of this reaction was around 0.6 mol.%.

3.3. Microstructure

Fig. 6 shows the SEM photographs of the YDC0Zn, YDC0.6Zn and YDC0.8Zn sintered at 1375 °C. The sample of YDC0Zn was found to be very porous. The pores are continuous and open. In contrast, the sample of YDC0.6Zn was well dense, which is in agreement with the shrinkage and density results above. For YDC0.8Zn, it is interesting that grains of two different sizes were observed. The specimen includes a substrate of smaller grains with closed pores at multiple junctions and some isolated conglomeration of larger grains on the surface. According to the energy dispersive spectroscopy (EDS) results shown in Fig. 7, the bottom layer was cerium-rich region, while the "floating" large particles were zinc-rich. The mechanism of this special microstructure is still under research, but we may

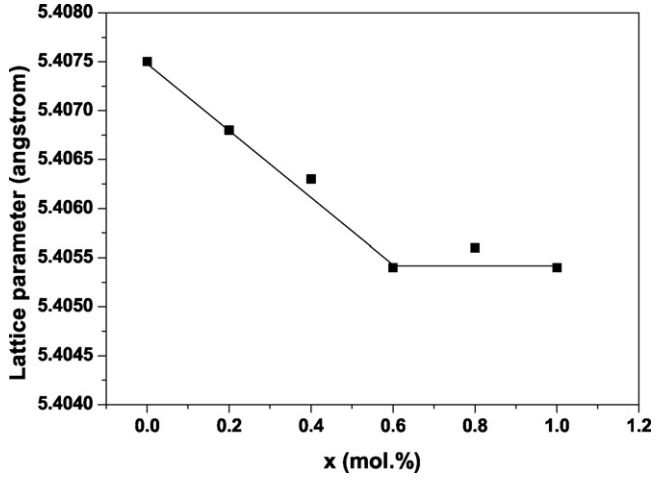

Fig. 5. Lattice parameter derived from the XRD pattern vs. zinc oxide content.

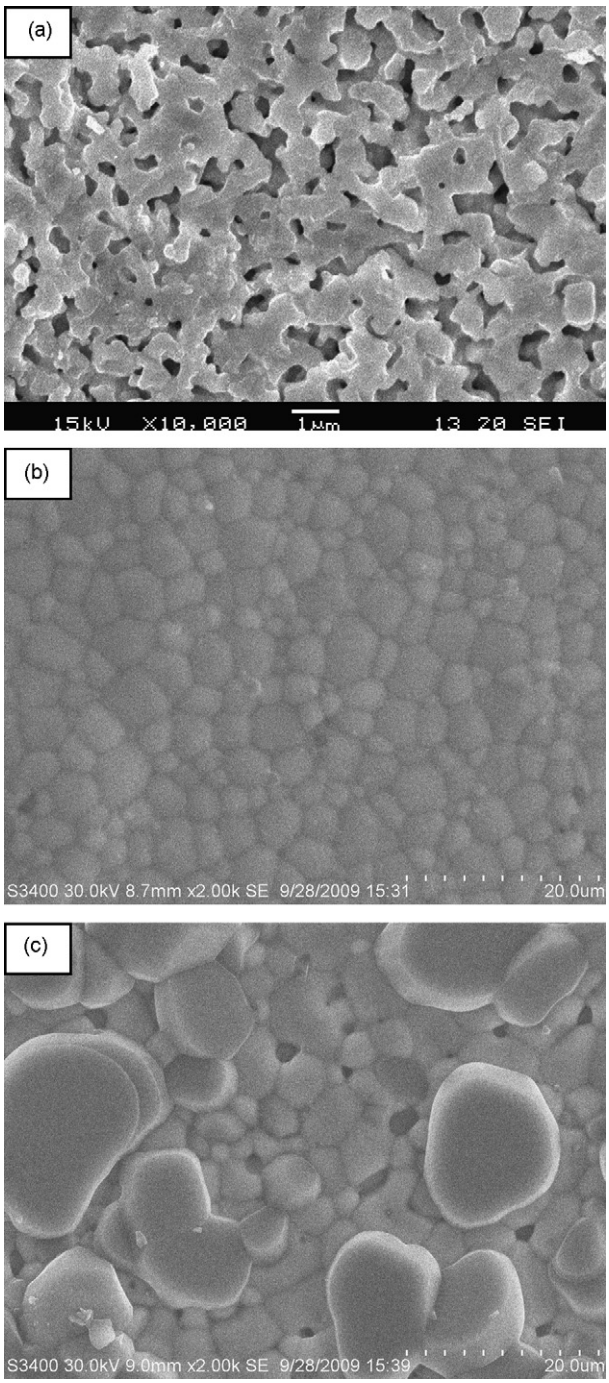

Fig. 6. SEM photographs of YDC0Zn (a), YDC0.6Zn (b) and YDC0.8Zn (c) sintered at 1375 °C for 20 h in air.

speculate that, when the addition of zinc oxide exceeds the solubility limit, the excess part has a tendency to agglomerate and locate on the surface of the sample after sintering.

3.4. Electrical conductivity

The ionic conductivity of $(Ce_{0.84}Y_{0.16}O_{1.92})_{1-x}(ZnO)_x$ was measured by means of two probe AC impedance spectroscopy. The contributions of grain interior, grain boundary and electrode–electrolyte were represented by three equivalent circuit units, of which consist parallel resistance and constant phase element (CPE). Replacing capacitance by CPE, accounts for the inhomogeneity of microstructure within the sintered samples.

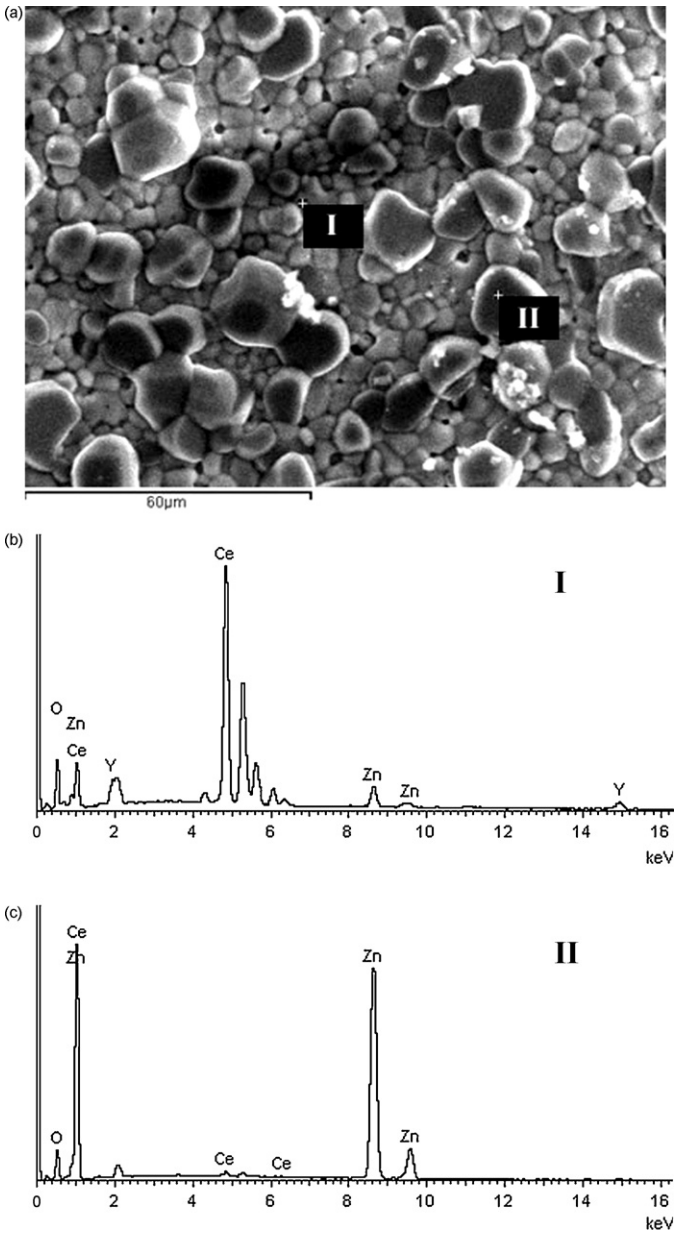

Fig. 7. EDS results of YDC0.8Zn sintered at 1375 °C for 20 h in air.

The total resistance of electrolyte can be expressed as:

$$R_t = R_{gi} + R_{gb} \quad (3)$$

where R_{gi} is the resistance of grain interior and R_{gb} is the resistances of grain boundary. They are both obtained by fitting the impedance data. Then the total conductivity could be calculated from the equation:

$$\sigma_t = \frac{d}{SR_t} \quad (4)$$

where d is the thickness of the sample and S is the area of electrode.

Fig. 8 shows the resistance of grain interior and grain boundary from the impedance spectroscopy measured at 350 °C. The R_{gi} of all four specimens fluctuate slightly around 125 Ω. However, the R_{gb} of YDC0.8Zn rapidly increases compared with that of YDC0.6, which implies that the redundant ZnO accumulated at the grain boundary did negative effect on the migration of oxygen ions.

Fig. 9 shows the temperature dependence of conductivities of ZnO doped YDC samples sintered at 1375 °C. As a contrast, data

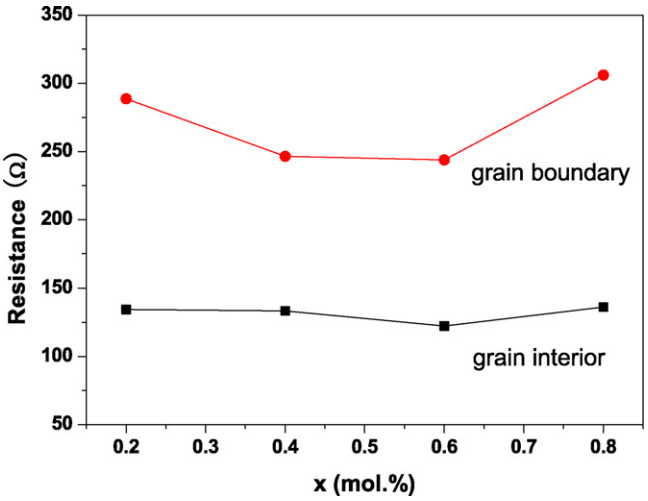

Fig. 8. Resistances of grain interior and grain boundary derived from impedance spectroscopy vs. zinc oxide contents.

of dense YDC0Zn sample sintered at 1600 °C were also included. Compared with other doped samples, the ionic conductivity of YDC0.6Zn was observed to be mostly close to the value of YDC0Zn, only 1.7% lower. Below ZnO solubility limit ($x \leq 0.6$ mol.%), the ionic conductivity of doped specimens was in proportion to the ZnO content due to the domination of excess oxygen vacancies; and above the limit ($x > 0.6$ mol.%), the increasing second phase of ZnO deteriorated the electrochemical property.

Fig. 10 shows the relationship between $\ln \sigma T$ and the reciprocal of temperature. The data all well obey the Arrhenius equation:

$$\sigma = \frac{A}{T} \exp\left(-\frac{E_a}{kT}\right) \quad (5)$$

where A is the pre-exponential factor, T is the absolute temperature, E_a the activation energy for ionic migration and k is the Boltzmann constant.

Fig. 11 presents the calculated activation energy as a function of ZnO doping level. We presumed the relatively higher overall activation energy of YDC0.2Zn was attributed to the condition of its grain boundary phase as the density of the specimen is relatively lower. Within the solid solubility limit, the E_a value of YDC0.6Zn (0.7067 eV) is slightly higher than that of YDC0.4Zn (0.7062 eV). Moreover, both of the values are higher than that of YDC0Zn sintered at 1600 °C (0.7007 eV). It is suggested that the charged

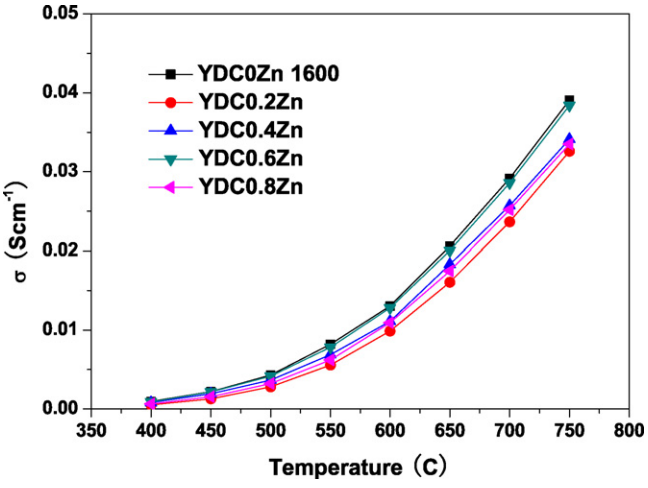

Fig. 9. Total conductivities vs. testing temperature for YDC with different zinc oxide contents.

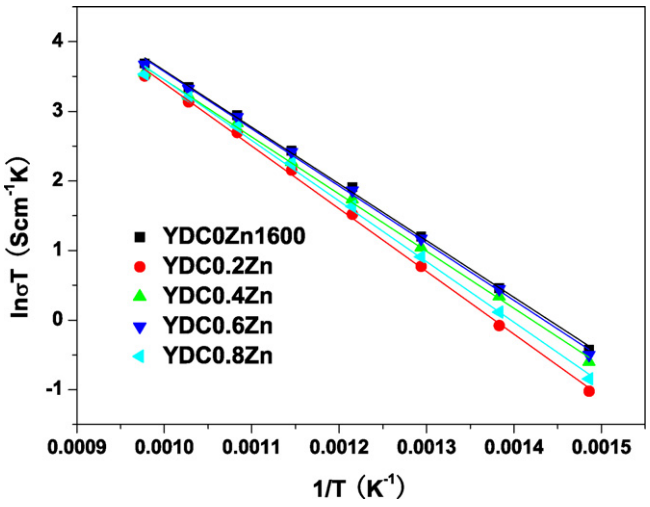

Fig. 10. Arrhenius plot of YDC with different zinc oxide contents.

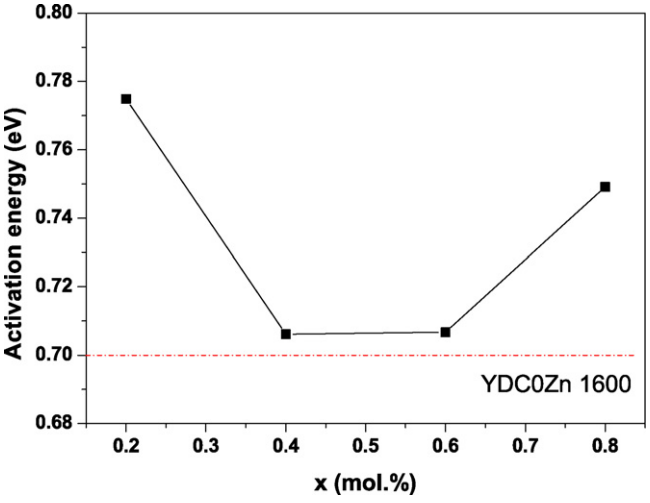

Fig. 11. Activation energy as a function of zinc oxide content.

substituted zinc sites may attract with the ambient oxygen vacancies. *i.e.*

$$Zn''_{Ce} + V_O^{\bullet\bullet} \leftrightarrow (Zn''_{Ce} \cdot V_O^{\bullet\bullet})^{\times} \quad (6)$$

This kind of attraction increases with the dissolved ZnO content because of the increasing Zn''_{Ce} and compact lattice matrix.

4. Conclusion

As an effective sintering aid, ZnO is able to lower the sintering temperature of YDC electrolyte from ~1600 °C to 1375 °C. Approximately 0.6 mol.% zinc could dissolve into the cubic fluorite structure of YDC according to the result of XRD analysis. The EDS revealed that further addition of zinc oxide will result in the existence of second phase. The optimum composition is observed at YDC0.6Zn, whose ionic conductivity is mostly close to pure YDC sintered at 1600 °C. The insignificant loss was presumed to result from the defect bonding of substituted zinc sites with their surrounding oxygen vacancies.

Acknowledgement

We acknowledge support of Analysis Center of Nanjing University and State Key Laboratory of Material-Oriented Chemical Engineer.

References

[1] N.Q. Minh, J. Am. Ceram. Soc. 76 (3) (1993) 563–588.
[2] B.C.H. Steele, A. Heinzel, Nature 414 (2001) 345–352.
[3] H. Yahiro, K. Eguichi, H. Arai, Solid State Ionics 36 (1989) 71–75.
[4] K. Eguchi, T. Setoguchi, T. Inoue, H. Arai, Solid State Ionics 52 (1992) 165–172.
[5] G. Bryan Balazs, R.S. Glass, Solid State Ionics 76 (1995) 155–162.
[6] C. Tian, S. Chan, Solid State Ionics 134 (2000) 89–102.
[7] H. Yoshida, K. Miura, T. Fukui, S. Ohara, T. Inagaki, J. Power Sources 106 (2002) 136–141.
[8] W. Lai, S.M. Haile, J. Am. Ceram. Soc. 88 (11) (2005) 2979–2997.
[9] S. Kuharuangrong, J. Power Sources 171 (2007) 506–510.
[10] E.Yu. Pikalova, V.I. Maragou, A.N. Demina, A.K. Demin, P.E. Tsiakaras, J. Power Sources 181 (2008) 199–206.
[11] C.M. Lapa, D.P. Ferreira de Souza, F.M.L. Figueiredo, F.M.B. Marques, J. Power Sources 187 (2009) 204–208.
[12] D.Y. Wang, D.S. Park, J. Griffith, A.S. Nowick, Solid State Ionic 2 (1981) 95–105.
[13] R.T. Dirstine, R.N. Blumenthal, T.F. Kuech, J. Electrochem. Soc 126 (1979) 264–269.
[14] C. Pascual, J.R. Jurado, G.F. Arroyo, L. Del Olmo, C. Moure, P. Duran, Sci. Ceram. 12 (1984) 729–734.
[15] T.S. Zhang, J. Ma, H.T. Huang, P. Hing, Z.T. Xia, S.H. Chan, J.A. Kilner, Solid State Sci. 5 (2003) 1505–1511.
[16] C. Kleinlogel, L.J. Gauckler, Solid State Ionics 135 (2000) 567–573.
[17] T.S. Zhang, J. Ma, L.B. Kong, P. Hing, Y.J. Leng, S.H. Chan, J.A. Kilner, J. Power Sources 124 (2003) 26–33.
[18] T.S. Zhang, P. Hing, H. Huang, J. Kilner, Mater. Lett. 57 (2002) 507–512.
[19] T.S. Zhang, L.B. Kong, Z.Q. Zeng, H.T. Huang, P. Hing, Z.T. Xia, J. Kilner, J. Solid State Electrochem. 7 (2003) 348–354.
[20] T.S. Zhang, Z.Q. Zeng, H.T. Huang, P. Hing, J.A. Kilner, Mater. Lett. 57 (2002) 124–129.
[21] M. Mori, E. Suda, B. Pacaud, K. Murai, T. Moriga, J. Power. Sources 157 (2006) 688–694.
[22] J. Van herle, T. Horita, T. Kawada, N. Sakai, H. Yokokawa, M. Dokiya, Solid State Ionics 86–88 (1996) 1255–1258.
[23] J. Van herle, T. Horita, T. Kawada, N. Sakai, H. Yokokawa, M. Dokiya, J. Am. Ceram. Soc. 80 (4) (1997) 933–940.
[24] C. Tian, S. Chan, Solid State Ionics 134 (2000) 89–102.
[25] S.K. Tadokoro, T.C. Porfirio, R. Muccillo, E.N.S. Muccillo, J. Power Sources 130 (2004) 15–21.
[26] H. Xu, H. Yan, Z. Chen, J. Power Sources 163 (2006) 409–414.
[27] H.M. Xu, H.G. Yan, Z.H. Chen, Mater. Charact. 59 (2008) 301–305.
[28] T. Van Dijk, A.J. Burggraaf, Phys. Status Solidi (a) 63 (1981) 229–240.
[29] R.D. Shannon, Acta Cryst. A32 (1976) 751–767.